



# Pulse plating of Ni–Mo alloys from Ni-rich electrolytes

A. Marlot, P. Kern, D. Landolt <sup>\*,1</sup>

*Materials Institute-LMCH, Swiss Federal Institute of Technology Lausanne, CH-1015 Lausanne EPFL, Switzerland*

Received 14 June 2002; received in revised form 21 August 2002

## Abstract

Pulse plating of Ni–Mo alloys from nickel-rich electrolytes was studied with an inversed rotating disk electrode. The deposit composition and the current efficiency were measured as a function of pulse variables (pulse period, duty cycle) and mass transport parameters (electrode rotation speed, molybdate concentration). At sufficiently short pulse periods, the Mo content of the pulse plated alloys was higher than in dc plating. Experiments using a rotating electrochemical quartz crystal microbalance and Auger electron spectroscopy showed that under the conditions of the experiments no significant corrosion reaction takes place during the pulse off-time. A simplified non-steady state diffusion model can explain the observed enhancement in Mo content and correctly predict the influence of pulse plating variables on deposit composition.

© 2002 Elsevier Science Ltd. All rights reserved.

*Keywords:* Nickel–molybdenum alloys; Pulse plating; Mass transport; Induced codeposition

## 1. Introduction

Electrodeposited nickel/molybdenum alloys are interesting materials due to their high corrosion resistance and low hydrogen overpotential. From a theoretical point of view, electrodeposition of these alloys is an example of the so-called induced codeposition mechanism [1]. Pure molybdenum cannot be electrodeposited from aqueous solutions, but it can be codeposited with an iron group metal forming an alloy. The induced codeposition of molybdenum with nickel, cobalt or iron has been investigated in our laboratory using direct current (dc) plating [2–4]. A reaction model was proposed to explain the codeposition mechanism. It involves an adsorbed nickel–molybdenum intermediate, the formation of which requires the presence of nickel ionic species at the electrode surface. Molybdenum deposition proceeds through the mixed reaction intermediate while nickel deposition takes place by the usual two steps mechanism. Depending on relative concentrations, mass transport of either molybdate or nickel may

limit the deposition rate of molybdenum and therefore, control the alloy composition. The model was found to correctly predict the influence of the electrode rotation rate and the imposed potential on the current efficiency (CE) and the alloy composition.

Compared to dc plating, pulse current (pc) techniques offer several advantages such as the availability of additional process parameters which can be varied independently and the possibility of achieving higher instantaneous current densities [5–9]. Pulse plating has proved to be an important technology for improving the properties of deposits [10]. It can also produce alloy compositions and microstructures which are not obtainable with dc plating techniques [11,12]. Several studies of pulse plated Ni–Mo and similar alloys are reported in the literature [13–17]. Most investigations were aimed at improving the quality of the alloy layers and they report the influence of pulse parameters on deposit composition, CE and physical properties. To the authors' knowledge, a quantitative understanding of how pulse variables affect the composition of Ni–Mo alloys is still lacking.

Previous studies have shown that corrosion processes during the off-time can significantly influence the composition of pulse plated alloys. Auger electron spectroscopy (AES) analysis [18] or in situ measure-

\* Corresponding author. Tel.: +41-21-693-2981; fax: +41-21-693-3946

E-mail address: dieter.landolt@epfl.ch (D. Landolt).

<sup>1</sup> ISE member.

ments with an electrochemical quartz crystal microbalance (EQCM) [19] were used by several authors to detect these processes. For Cu–Ni codeposition, Roy et al. [18,20] found that the composition of the pulse plated alloy was governed by a displacement during the off-time of the less noble nickel by the more noble copper. For the interpretation of their experimental results, these authors developed two models assuming the occurrence or not of a corrosion reaction. Depending on the length of the pulse off-time one or the other model gave a better description of the observed behavior. Mass transport plays an important role in pulse plating [21]. The influence of pulse parameters on alloy composition for a system where one component deposits under diffusion control and the other under activation control has been discussed theoretically using the duplex diffusion layer approach introduced by Ibl [6,22] for single component systems. Dossenbach et al. [23] used the same approach to explain composition changes in pulse plated Ag–Pd alloys. Yang and Cheh [24,25] took into account instantaneous current densities during pulse plating to predict the composition of copper/nickel multilayers.

The aim of the present study is to contribute to a better understanding of the effect of pulse plating parameters on the composition of Ni–Mo alloys electrodeposited from nickel rich ammonia citrate electrolytes. In particular the role of corrosion processes and non-steady state diffusion effects will be studied. The composition of deposits and the CE are measured for different pulse parameters (pulse time, pulse period and duty cycle) and mass transport conditions (electrode rotation rate and electrolyte concentrations). AES and EQCM experiments are conducted to substantiate electrochemical data. Experimental results are compared to simplified theoretical approaches.

## 2. Experimental

Ni–Mo deposits were prepared for compositional analysis using an inverted rotating disk electrode (IRDE) described in detail elsewhere [26]. This electrochemical cell permits a good control of the plating process including the choice of substrate, evacuation of hydrogen, uniform mass transport and current distribution. Substrates used in this study were bulk copper disks (99.99%, Goodfellow, England). Before each experiment, the working electrodes were polished to a near mirror finish and ultrasonically cleaned with ethanol. The working electrode exposed area was 0.50 cm<sup>2</sup>. Pulse plating experiments were conducted using a Heka potentiostat (PG 390 Heka Elektronik GmbH, Germany) controlled by a Labview program. The reference electrode was a sulfate mercurous electrode (Radiometer, France). A dimensionally stable anode

(Eltech Systems Corp., USA) served as the counter-electrode. It was placed in a compartment separated by a glass frit of porosity 4. The electrode rotation speed was controlled by a modulated speed rotator (Pine Instrument Company, USA) and ranged between 300 and 1500 rpm. A charge of 8 C cm<sup>-2</sup> was passed for each experiment. The deposit thickness was 1–1.5 μm. For all experiments, the on-time ( $i_p$ ) and off-time ( $i_p'$ ) current densities were  $-50$  and  $-0.03$  mA cm<sup>-2</sup>, respectively. This off-time current density value was the closest to zero that could be achieved with the electrochemical set-up, while remaining slightly cathodic. The duty cycle ( $\gamma$ ) was set at 0.2, 0.4 or 0.6. The pulse period ( $t_{pp}$ ) was ranging from 1 ms to 50 s.

An ammonia citrate electrolyte was used containing 0.7 M NiSO<sub>4</sub>, 5 mM Na<sub>2</sub>MoO<sub>4</sub>, 0.8 M Na<sub>3</sub>Cit and 0.28 M NH<sub>3</sub>. For some experiments the sodium molybdate concentration was varied between 5 and 20 mM. The solutions were deaerated with nitrogen for 1 h before experiments. The N<sub>2</sub> flux was maintained above solution during deposition. All experiments were conducted at 25 °C.

CE measurements were performed on bulk Ag cylinder substrates (99.95%, Goodfellow, England) using a rotating cylinder cell. The working electrode area was 4.0 cm<sup>2</sup> (H 13 mm, Ø 10 mm). The plating conditions with the rotating cylinder electrode (RCE) were the same as described for the IRDE. The rotation rates were chosen to yield the same diffusion layer thickness as the RDE experiments [27]. The Ag substrates were prepared the same way as the Cu disks. For each experiment, the passed charge was 8 C cm<sup>-2</sup> yielding a deposit mass of around 5 mg. Weight measurements were performed using a balance Sartorius 2004 MP6 sensitive to 0.01 mg.

Some deposits were prepared using a rotating EQCM described in detail elsewhere [28]. Substrates were 10 MHz AT-cut quartz crystals covered with gold electrodes. The working electrode area was 0.203 cm<sup>2</sup>. Experiments were conducted with a Zahner potentiostat (model IM6, Zahner, Germany) and a PC acquiring data at a frequency of 10, 100 or 500 Hz. A mercurous sulfate reference electrode (Radiometer, France) and a Pt coil counter electrode were used. The rotation speed of the working electrode, controlled by a speed control unit (CTV101, Radiometer, France), was 1000 rpm for all experiments. For reproducibility, an approximately 100 nm Ni–Mo layer was first deposited on gold at  $-1.55$  V/MSE. Five pulse cycles were recorded after 25 prior pulse cycles. This was found to be necessary to approach steady-state pulse plating conditions. The duty cycle was 40% and the pulse period was either 500 ms or 20 s. The on-time current density was  $-50$  mA cm<sup>-2</sup>. The electrolyte contained 0.35 M nickel sulfate, 5 mM sodium molybdate, 0.4 M sodium citrate and 0.28 M ammonia. The pH was equal to 8.5.

Solutions were deaerated for 1 h before experiments and maintained at 25 °C.

The composition of the deposits was determined with a Kevex Omicron X-ray fluorescence (XRF) analyzer calibrated with bulk samples of nickel and molybdenum. Five measurements were taken on the center region of Cu substrates with a 300  $\mu\text{m}$  collimator. The variation in alloy composition for a given sample was less than  $\pm 2\%$ . The surface morphology of some deposits was studied by scanning electron microscopy (SEM) using a JEOL 6300F microscope.

AES depth profiling was performed with a Perkin–Elmer 660 scanning Auger microprobe system. A primary electron beam current of 150 nA at 5 keV was employed. Sputtering was carried out using a 2 keV Ar ion beam rastered over an area of  $2 \times 2 \text{ mm}^2$ . The sputter rate of a  $\text{Ta}_2\text{O}_5$  thin film standard was  $17.5 \text{ \AA min}^{-1}$  for these conditions. After pulse deposition on IRDE, the current was switched off and the sample isolated from the solution. It was then removed from the cell, rinsed with distilled water and dried with argon. It was placed in a vacuum chamber of  $10^{-7}$  torr pressure until the AES measurement was carried out. To investigate corrosive properties of the electrolyte, some samples were let in solution after deposition for 30 min before AES measurements.

### 3. Results

In Fig. 1a the measured molybdenum content in deposits is plotted as a function of pulse period ( $t_{pp}$ ) for different duty cycles. The pulse period was varied between 1 ms and 50 s by changing both the pulse on-time and off-time. Three series of experiments were conducted using three different duty cycles. The average current density was 10, 20 or  $30 \text{ mA cm}^{-2}$  when the duty cycle was set at 0.2, 0.4 or 0.6 respectively. A slight increase of the Mo content is first observed when the pulse period is progressively increased from 1 ms to 30 ms, except for experiments conducted with a duty cycle of 0.2. At higher pulse periods, all curves show a significant decrease of the Mo content with increasing  $t_{pp}$ . As an example, deposits prepared with an average current density of  $20 \text{ mA cm}^{-2}$  contained around 25% of molybdenum when the pulse period was fixed to 30 ms and 10% when this variable was increased up to 10 s. At pulse periods above 10 s, the Mo content in the alloys was constant, independent from duty cycle and corresponded to the composition of deposits prepared by dc plating at the same current density  $i_p$  (10%). On the other hand, Fig. 1a shows that duty cycle affects the alloy composition at pulse periods below 10 s. Under such conditions, a lower duty cycle leads to an enhancement of the Mo content in the alloy. As an example, the Mo content in alloys prepared at 30 ms can

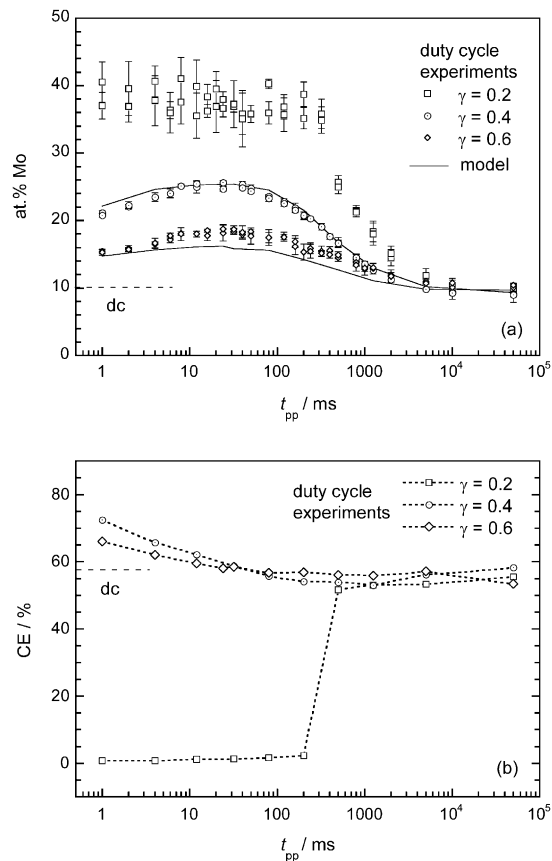


Fig. 1. Variation of the Mo content (a) and the cathode efficiency (b) as a function of pulse period. Deposits were prepared with various duty cycle values. The electrode rotation rate was 1000 rpm. Measured data (dots) and calculated curves are given. dc values are shown by a dashed line.

be increased from 18 to 38% by changing the duty cycle from 0.6 to 0.2.

Corresponding CE data are shown in Fig. 1b. Each point represents the mean value obtained from two experiments. Variations recorded with a duty cycle equal to 0.4 and 0.6 show very similar trends. The CE slightly decreases with increasing  $t_{pp}$  approaching the asymptotic value for dc (57%) at long pulse periods. Similar observations were reported by Eckler et al. [29] in their study of pc plated chromium–molybdenum alloys. Generally, the pulse plated alloy deposits were compact and homogeneous. Exceptions were noticed for alloys with a relatively high Mo content (around 38%) plated at  $\gamma = 0.2$  with a very low CE (less than 5%). These deposits were thin and non-compact.

Fig. 2 shows variations of both the Mo content and the CE as a function of sodium molybdate concentration in solution. The average current density was equal to  $20 \text{ mA cm}^{-2}$  and the pulse period set at 50 s. As observed with previous experiments, alloys with a relatively high Mo content were non-compact due to a very low deposition efficiency. When compact deposits were formed, both the Mo content and CE increased

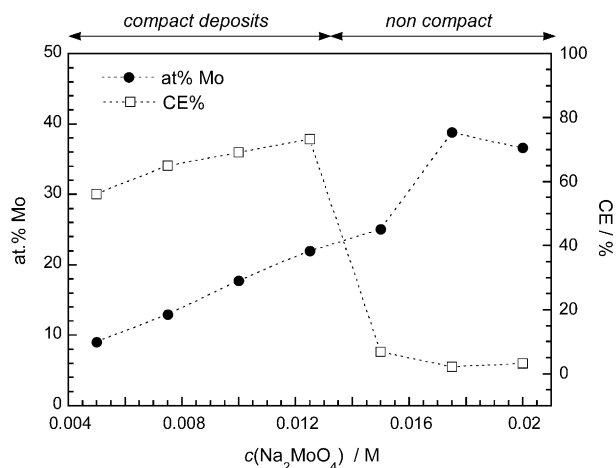


Fig. 2. Influence of the sodium molybdate concentration on the Mo content in alloys and CE. Deposits were plated at a pulse period of 50 s. The electrode rotation rate was 1000 rpm. Each dot represents the mean value estimated from two experiments.

with molybdate concentration in the electrolyte. This suggests that the codeposition process is limited by the diffusion of Mo(VI) in solution as observed previously by [2–4].

Additional experiments were conducted by changing the electrode rotation speed. Fig. 3 shows the measured alloy composition for two series of experiments performed with a pulse period of 50 s and 20 ms, respectively. In both cases, the Mo content in the deposits increases almost linearly with the electrode rotation speed except for non-compact deposits obtained at 20 ms at high rotation rates. For compact deposits, the variation of the Mo content with rotation speed depends on the pulse period.

To understand such effects, partial current densities were calculated from the data of Fig. 3. Results shown in Fig. 4 indicate that the partial current density of Mo

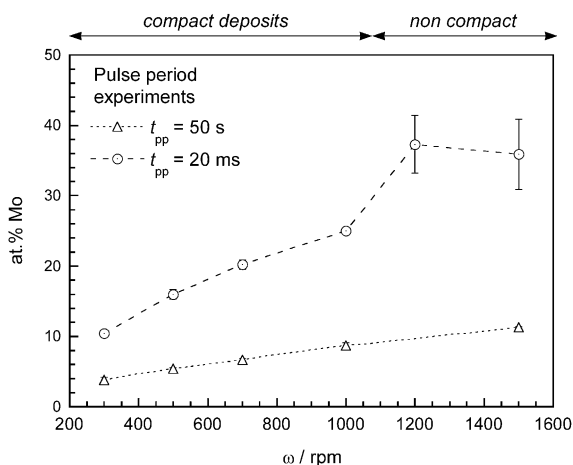


Fig. 3. Influence of the electrode rotation speed on the Mo content for deposits prepared at a pulse period of 20 ms or 50 s. The duty cycle was 0.4 and the electrode rotation rate 1000 rpm. Each dot represents the mean value estimated from two experiments.

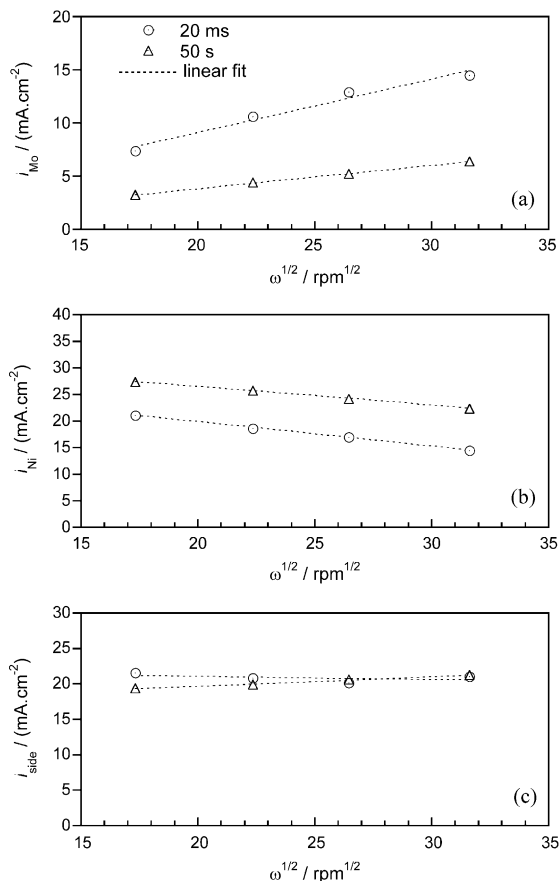


Fig. 4. Variations of the partial current densities calculated from data of Fig. 3 as a function of the square of the electrode rotation rate.

deposition ( $i_{\text{Mo}}$ ) increases linearly with  $\omega^{1/2}$  (Fig. 4a). The slope depends on pulse period and is higher at 20 ms. The side reaction current ( $i_{\text{side}}$ ) shown in Fig. 4c is almost constant and independent of  $\omega$ . A different behavior is observed for the Ni partial current (Fig. 4b) that significantly decreases with  $\omega^{1/2}$ .

In Fig. 5 are shown the SEM images of two Ni–Mo deposits prepared at an average current density of 20  $\text{mA cm}^{-2}$  with a pulse period of 12 ms (A) or 10 s (B). Deposits contained 25% and 9.4 at.% Mo, respectively. The electrode rotation speed was 1000 rpm. Both deposits have a globular surface texture. The similar surface morphology suggests that the observed effects of rotation rate and pulse period on Mo content (Figs. 3 and 4) are not related to structural or roughness effects.

Fig. 6 shows typical data recorded with the r-EQCM with a pulse period of respectively 20 s (a) and 0.5 s (b). The measured potential and the quartz frequency response are shown, along with the imposed current density. The change in quartz resonance frequency is related to the mass change of the electrode by the Sauerbrey equation:

$$\Delta m = -k\Delta f \quad (1)$$

This equation is applicable for small mass changes and

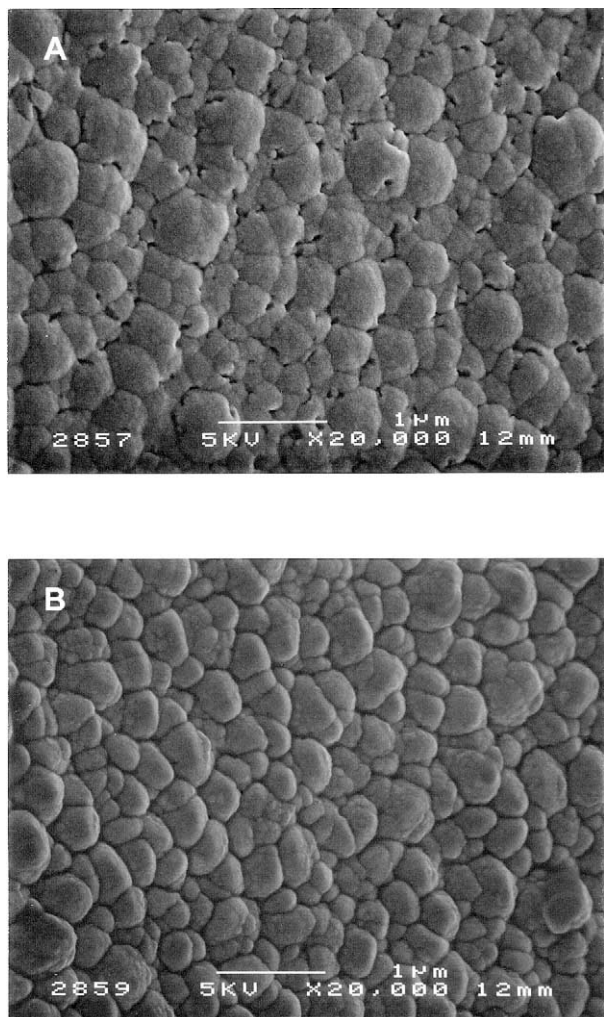


Fig. 5. SEM images of Ni–Mo deposits prepared with a pulse period of 12 ms (A) and 10 s (B). The duty cycle was 0.4 and the electrode rotation rate 1000 rpm.

layers rigidly attached to the quartz [30]. The proportionality constant  $k$  for the present experimental setup is  $0.213 \text{ Hz cm}^{-2} \text{ ng}^{-1}$  [28]. In Fig. 6a, the quartz response indicates the formation of the Ni–Mo deposit as the pulse current is switched on. The mass increases linearly with time. The slope  $+9.65 \pm 0.04 \mu\text{g cm}^{-2} \text{ s}^{-1}$  is very close to the value  $+9.19 \mu\text{g cm}^{-2} \text{ s}^{-1}$  determined from ex situ gravimetry and composition measurements. At a higher pulse frequency (Fig. 6b), the deposition of Ni–Mo alloys exhibits a short delay ( $\sim 15 \text{ ms}$ ) at the beginning of the pulse on-time that may be due to the double layer charging at the beginning of each pulse [10]. After this delay, the mass increases linearly with time. Due to the difference in the charge number and molecular mass between nickel and molybdenum ( $z_{\text{Ni}} = 2$ ,  $M_{\text{Ni}} = 58.69 \text{ g mol}^{-1}$ ,  $z_{\text{Mo}} = 6$ ,  $M_{\text{Mo}} = 95.94 \text{ g mol}^{-1}$ ), the mass gain is slightly lower ( $+8.87 \pm 0.07 \mu\text{g cm}^{-2} \text{ s}^{-1}$ ) for a pulse period of 0.5 s than for 20 s, as expected from the difference in composition shown in

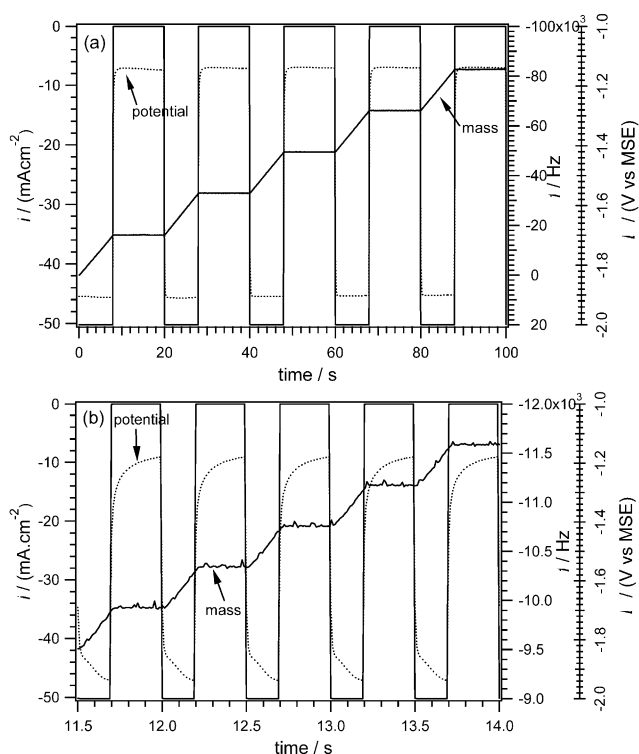


Fig. 6. r-EQCM frequency and potential responses for galvanostatic deposition at a pulse period of 20 s (a) 0.5 s (b). The square waveform is the applied current density while  $\Delta f$  and potential signals are as indicated.

Fig. 1a. No measurable mass change is observed during the pulse off-time. This indicates that no significant corrosion process took place.

To verify the absence of a displacement reaction during the off-time, AES experiments were conducted. Depth profiles for nickel, molybdenum and oxygen were measured for a dc plated deposit immediately removed from the solution after deposition (Fig. 7a) and after 30 min of immersion in the solution (Fig. 7b). The absence of a significant difference in the Ni and Mo profiles

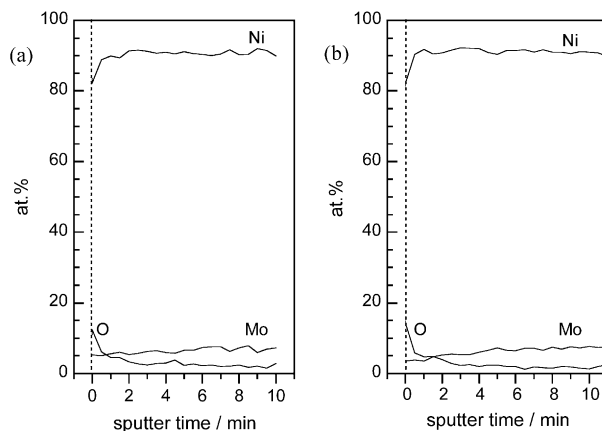


Fig. 7. AES depth profiles of a dc plated Ni–Mo alloy immediately removed from solution (a) or let for 30 min in solution (b) after deposition.

between Fig. 7a and b confirms that no significant displacement reactions took place during prolonged immersion. The oxygen signal at the deposit surface (sputter time less than 150 s) is attributed to air oxidation during sample transfer. Away from the surface the oxygen signal corresponds to the background noise, confirming the metallic nature of the deposit.

#### 4. Discussion

The present results illustrate the differences in behavior of the Ni–Mo system at short and long pulse periods. Above 10 s, the composition of Ni–Mo alloys is the same as that of dc plated deposits and independent of the pulse parameters (duty cycle and pulse period). The Mo content is controlled by steady state mass transport conditions (electrode rotation speed and molybdate concentration). At pulse periods below 10 s, the Mo content is significantly increased by the pc method and it depends on both pulse frequency and duty cycle besides rotation rate. An increase of the Mo content in pc plated deposits has previously been mentioned in the literature [14,16,17,29].

For certain alloy systems displacement reactions are known to affect the deposit composition in pulse plating [18,20]. Our AES and EQCM investigations show that such reactions are not relevant for Ni–Mo alloys. Capacitance effects are another important factor in pulse plating [6,10]. The charging time of the double layer depends on current density and other physical parameters of the system and it is usually well below a millisecond. Capacitive effects are therefore relevant only at very short pulse periods and cannot explain the composition variations in the pulse period range studied here.

It clearly appears from Fig. 4a and b that the codeposition process of Ni–Mo alloys under the present conditions is controlled by mass transport of Mo(VI) species in solution. In pulse electrolysis mass transport involves steady state and non-steady state processes. Several authors have developed mathematical models to describe these phenomena [5–9,21,31,32]. The most important quantity for mass transfer in pulse plating is the pulse limiting current density  $i_{pL}$ . It was defined as the limiting current density value for which the surface concentration becomes zero at the end of the pulse. It differs from the steady-state limiting current density  $i_L$  in dc plating. Cheh [7] gave an approximate solution for rectangular pulse forms and calculated the ratio  $i_{pL}/i_L$  for different conditions. He showed that at very small pulse periods the limiting value of the instantaneous limiting current can be considerably higher than the steady state limiting current due to the steeper concentration gradient. On the other hand, the limiting overall plating rate which involves an integration of the current

over the pulse period is always equal or lower than in dc deposition. A generalized mathematical model for arbitrary pulse forms was developed by Chin [9] who confirmed that applying a pulsed current can considerably increase (100–1000 times) the instantaneous limiting current density compared to that of dc plating. Ibl [6] introduced the concept of a pulsating diffusion layer and proposed a simple mathematical model to express  $i_{pL}$ . His approach was further developed by Datta and Landolt [31]. All these models apply to pure metal deposition and applied current pulses. Viswanathan et al. [32] numerically calculated the average current density under intermittent potential variations assuming the surface concentration of the reacting species to be always zero. They also developed approximate methods for the estimation of the upper and lower bounds of the numerical solution. The approximate model of Viswanathan et al. [32] can be applied to the present experiments by assuming that during codeposition from a Ni-rich electrolyte molybdate is reduced at its transport limited rate throughout the pulse on-time. The surface concentration of molybdate therefore is zero while the concentration gradient varies with time. Ni reduction on the other hand is entirely charge transfer controlled. Applied to molybdenum, the model of Viswanathan et al. [32] yields for the ratio of the average pulse limiting current density of molybdate during the pulse on-time  $\bar{i}_{pL,Mo}$  over its dc limiting current density  $i_{L,Mo}$ :

$$\begin{aligned} \frac{\bar{i}_{pL,Mo}}{i_{L,Mo}} \Big|_{\text{upper}} &= \frac{1}{\tau_{pp}} \left( \tau_p + \frac{1}{3} - \sum_{n=1}^{\infty} \frac{2}{\mu_n^2} \exp[-\mu_n^2(\tau_{pp} - \tau_p)] \right) \quad (2) \\ \frac{\bar{i}_{pL,Mo}}{i_{L,Mo}} \Big|_{\text{lower}} &= \left( \frac{\tau_p}{\tau_{pp}} \right) \\ &\times \left( 1 - 2 \sum_{n=1}^{\infty} \frac{1}{\mu_n^2} \frac{[\exp(-\mu_n^2 \tau_p) - \exp(-\mu_n^2 \tau_{pp})]}{[1 - \exp(-\mu_n^2 \tau_{pp})]} \right)^{-1} \quad (3) \end{aligned}$$

Here  $n$  is an integer and  $\mu_n$ , the coefficient  $\mu_n = (2n - 1)\pi/2$ .  $\tau_p$  and  $\tau_{pp}$  are the dimensionless pulse on-time and pulse period, respectively, defined by  $\tau_p = D_{Mo}t_p/\delta^2$  and  $\tau_{pp} = D_{Mo}t_{pp}/\delta^2$  where  $D_{Mo}$  is the diffusion coefficient of Mo(VI) species and  $\delta$ , the steady-state diffusion layer thickness on a rotating disk electrode [27]. To determine the diffusion coefficient  $D_{Mo}$ , Ni–Mo alloys were prepared by dc plating on RCEs at a current density of  $-50 \text{ mA cm}^{-2}$ . The value of  $D_{Mo}$  was calculated from the plot of the inverse of the partial Mo deposition current density as a function of the electrode rotation speed to the power  $-0.7$  (results not shown here), using the Eisenberg equation [33]. Its value was estimated to  $2.7 \times 10^{-6} \text{ cm}^2 \text{ s}^{-1}$  at  $25 \text{ }^\circ\text{C}$ , close to data given in Ref. [34].

Table 1  
Measured and computed Mo content (at.%) of Ni–Mo alloys pulse plated at different molybdate concentrations,  $t_{pp} = 50$  s

$c(\text{Na}_2\text{MoO}_4)$ (mM)	Measured (Fig. 2)	Calculated (Levich)	Calculated (Eq. (5))
5	9.0	9.8	9.7
7.5	13.0	13.4	13.3
10	17.7	18.0	18.0
12.5	22.0	22.6	22.7

The average dimensionless pulse limiting current density of molybdenum reduction during the pulse on-time is given by Eq. (4).

$$\overline{i_{pL,Mo}}^* = \frac{1}{2} \left( \overline{i_{pL,Mo}} \Big|_{i_{L,Mo} \text{ upper}} + \overline{i_{pL,Mo}} \Big|_{i_{L,Mo} \text{ lower}} \right) \quad (4)$$

In Fig. 8 is plotted the variation of  $\overline{i_{pL,Mo}}^*$  as a function of  $\tau_{pp}$  for different values of duty cycle. The computations indicate that high limiting current densities can be obtained by decreasing the value of either  $t_{pp}$  or  $\gamma$ . At very high pulse periods, the pulse limiting current density approaches the steady state value.

Based on this approach, the composition of pulse plated Ni–Mo alloys can be calculated using Eq. (5) and assuming that molybdenum is deposited at its average pulse limiting current density  $\overline{i_{pL,Mo}}^*$  during the overall pulse on-time. Experimental CE ( $\varepsilon$ ) values were used for the computations.

$$X_{Mo} = \frac{\overline{i_{pL,Mo}}^*}{3\varepsilon \times i_p - 2 \times \overline{i_{pL,Mo}}^*} \quad (5)$$

Tables 1 and 2 compare calculated data with the experimental results of Figs. 2 and 3. Only conditions where homogeneous and compact deposits were obtained are considered. When pulse period is sufficiently long (i.e. 50 s) steady state mass transport conditions are achieved during the pulse on-time. The composition of deposited films can then be simply calculated using the Levich equation [27] for  $i_{L,Mo}$ . All the results in Tables 1 and 2 show a good agreement between measurements and data calculated from the Viswanathan model. Eq.

Table 2  
Measured and computed Mo content (at.%) at different rotation rates

$\omega$ (rpm)	$t_{pp} = 50$ s		$t_{pp} = 20$ ms	
	Measured (Fig. 3)	Calculated	Measured (Fig. 3)	Calculated
300	3.8	4.4	10.4	13.0
500	5.4	6.0	16.0	17.1
700	6.7	7.5	20.2	20.5
1000	8.7	9.5	25.0	27.2
1500	11.3	13.7	–	–

Data were calculated with Eq. (5).

(5) can also be used to predict the effect of pulse variables (pulse period and duty cycle) on deposit composition (Fig. 1a). As expected from Fig. 8, non-steady state mass transport effects increase at small duty cycles and short pulse periods. Computed curves fit well experimental results obtained for compact deposited films. Nevertheless, this model cannot predict the effect of pulse parameters on CE and explain the observed upper value of Mo content in pc plated Ni–Mo deposits (38 at.%). More detailed numerical simulations including these effects are at present in progress.

## 5. Conclusions

The results of the present study show that the Mo content in Ni–Mo alloys plated from an electrolyte containing an excess of nickel can be increased in comparison with dc plating due to the higher instantaneous limiting current density of Mo. This effect is noticeable at sufficiently short pulse periods and for a codeposition process controlled by mass transport. At high pulse periods, diffusion current densities are the same as under dc conditions and the pulse current does not affect the composition. The absence of displacement reactions during the off-time has been verified. A simple mathematical approach has been used to describe

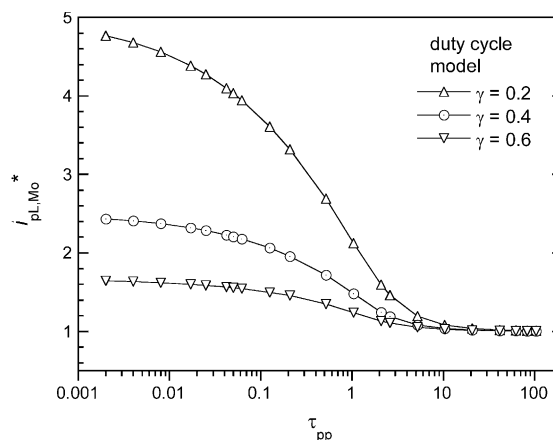


Fig. 8. Dimensionless average pulse limiting current density of molybdenum as a function of the dimensionless pulse period calculated for different duty cycles.

quantitatively the influence of pulse variables and convection parameters upon the composition of pulse plated Ni–Mo alloys

## 6. List of symbols

dc	direct current
$D$	diffusion coefficient ( $\text{cm}^2 \text{s}^{-1}$ )
$i_{\text{avg}}$	average current density ( $= \gamma i_p$ ) ( $\text{mA cm}^{-2}$ )
$i_L$	limiting (steady state) current density ( $\text{mA cm}^{-2}$ )
$i_p$	pulse current ( $\text{mA cm}^{-2}$ )
$i_{\text{pL}}$	limiting pulse current density ( $\text{mA cm}^{-2}$ )
$i_{\text{pL}}$	average limiting pulse current density during the pulse on-time ( $\text{mA cm}^{-2}$ )
$i_{\text{pL}}^*$	dimensionless limiting pulse current density
$i_{\text{pL}}^*$	dimensionless average limiting pulse current density during the pulse on-time
$k$	mass sensitivity of the quartz resonator ( $0.213 \text{ Hz ng}^{-1} \text{ cm}^{-2}$ )
$M$	molar weight ( $\text{g mol}^{-1}$ )
pc	pulse current
$t_p$	pulse on-time (s)
$t'_p$	pulse off-time (s)
$t_{\text{pp}}$	pulse period (s)
$X_{\text{Mo}}$	molar fraction of molybdenum in the deposit
$z$	number of electrons transferred in an electrochemical reaction
$\delta$	steady-state diffusion layer thickness ( $\mu\text{m}$ )
$\varepsilon$	CE
$\gamma$	duty cycle ( $= t_p/t_{\text{pp}}$ )
$\mu_n$	constant
$\tau_p$	dimensionless pulse on-time
$\tau_{\text{pp}}$	dimensionless pulse period
$\omega$	electrode rotation speed (rpm)
$\Delta f$	shift in the quartz crystal resonance frequency (Hz)
$\Delta m$	mass change ( $\text{ng cm}^{-2}$ )

## Acknowledgements

Financial support by the Fonds National Suisse de la Recherche Scientifique (Bern, Switzerland) is acknowledged.

## References

- [1] A. Brenner, *Electrodeposition of Alloys*, vol. 1–2, Academic Press, New York, 1963.
- [2] E.J. Podlaha, D. Landolt, *J. Electrochem. Soc.* 143 (1996) 885.
- [3] E.J. Podlaha, D. Landolt, *J. Electrochem. Soc.* 143 (1996) 893.
- [4] E.J. Podlaha, D. Landolt, *J. Electrochem. Soc.* 144 (1997) 1672.
- [5] N. Ibl, J.C.I. Puipe, H. Angerer, *Surf. Technol.* 6 (1978) 287.
- [6] N. Ibl, *Surf. Technol.* 10 (1980) 81.
- [7] H.Y. Cheh, *J. Electrochem. Soc.* 118 (1971) 551.
- [8] K. Viswanathan, M.A. Farrell Epstein, H.Y. Cheh, *J. Electrochem. Soc.* 125 (1978) 1772.
- [9] D.-T. Chin, *J. Electrochem. Soc.* 130 (1983) 1657.
- [10] J.-C.I. Puipe, F. Leaman (Eds.), *Theory and Practice of Pulse Plating*, AESF Society, Orlando, FL, 1986.
- [11] T. Nakanishi, et al., *J. Electrochem. Soc.* 148 (2001) C627.
- [12] J.J. Kelly, M. Cantoni, D. Landolt, *J. Electrochem. Soc.* 148 (2001) C620.
- [13] M. Cherkaoui, E. Chassaing, K. Vu Quang, *Plat. Surf. Finish.* 74 (1987) 50.
- [14] C.C. Nee, W. Kim, R. Weil, *J. Electrochem. Soc.* 135 (1988) 1100.
- [15] E. Chassaing, M.P. Roumegas, M.F. Trichet, *J. Appl. Electrochem.* 25 (1995) 667.
- [16] E. Beltowska-Lehman, P. Ozga, E. Chassaing, *Surf. Coat. Technol.* 78 (1996) 233.
- [17] M. Donten, Z. Stojek, *J. Appl. Electrochem.* 26 (1996) 665.
- [18] S. Roy, D. Landolt, *J. Electrochem. Soc.* 142 (1995) 3021.
- [19] J.J. Kelly, P. Kern, D. Landolt, *J. Electrochem. Soc.* 147 (2000) 3725.
- [20] S. Roy, M. Matlosz, D. Landolt, *J. Electrochem. Soc.* 141 (1994) 1509.
- [21] D. Landolt, in: J.-C.I. Puipe, F. Leaman (Eds.), *Theory and Practice of Pulse Plating* (Chapter 5), AESF Society, Orlando, FL, 1986.
- [22] D. Landolt, *Oberfläche-Surf.* 6 (1984) 25.
- [23] O. Dossenbach, B. Sturzenegger, J.-C. Puipe, *Oberfläche-Surf.* 9 (1987) 16.
- [24] C.C. Yang, H.Y. Cheh, *J. Electrochem. Soc.* 142 (1995) 3034.
- [25] C.C. Yang, H.Y. Cheh, *J. Electrochem. Soc.* 142 (1995) 3040.
- [26] P.E. Bradley, D. Landolt, *J. Electrochem. Soc.* 144 (1997) L145.
- [27] J.S. Newman, *Electrochemical Systems*, 2nd ed., Prentice Hall, Englewood Cliffs, NJ, 1991.
- [28] P. Kern, D. Landolt, *J. Electrochem. Soc.* 147 (2000) 318.
- [29] T.A. Eckler, B.A. Manty, P.L. McDaniel, *Plat. Surf. Finish.* 9 (1980) 60.
- [30] S. Bruckenstein, M. Shay, *Electrochim. Acta* 30 (1985) 1295.
- [31] M. Datta, D. Landolt, *Surf. Technol.* 25 (1985) 97.
- [32] K. Viswanathan, H.Y. Cheh, G.L. Standart, *J. Appl. Electrochem.* 10 (1980) 37.
- [33] M. Eisenberg, C.W. Tobias, C.R. Wilke, *J. Electrochem. Soc.* 101 (1954) 306.
- [34] Y. Zeng, et al., *Chin. J. Chem.* 18 (2000) 29.